

# Preparation and characterization of nanostructured Cu-doped ZnO thin film

H. EL MAROUAZI<sup>a,\*</sup>, A. EL HICHOUB<sup>b</sup>

<sup>a</sup>*Institut de Chimie et des Procédés pour l'Energie, l'Environnement et la Santé, CNRS/Université de Strasbourg, 25, rue Becquerel 67087 Strasbourg Cedex 2, France*

<sup>b</sup>*IMED-Lab. : Groupe d'Étude des Matériaux Optoélectroniques (G.E.M.O), Faculté des Sciences et Techniques, Université Cadi Ayyad, Av. A. Elkhatabi, BP 549, 40000 Marrakech, Morocco*

A sol-gel deposition route combined with a spin-coating process was utilized to fabricate undoped and doped Zinc oxide thin films on glass substrates with different copper concentrations ranging between 0 % and 10 mol%. XRD, SEM, and UV-vis spectral investigations were used to illustrate the structural features and optical behavior. The structural properties of ZnO films were directly influenced by copper doping. The variation of the copper ratio leads to the different behavior of all films' structural features. Moreover, the optical properties of all copper doped films confirm two distinct regions around 5 % of Cu. In conclusion, a copper doping concentration ratio higher than 5 % deteriorates all the films' structural and optical properties, suggesting that 5% of Cu is the maximum doping ratio. In comparison, 3% of Cu (where  $E_g = 3.240$  eV) was the optimum sample for practical applications like transparent conductive oxide (TCO).

(Received April 4, 2022; accepted June 9, 2023)

**Keywords:** Zinc oxide, Copper, Sol-gel, Coating, Thin films, Optical properties

## 1. Introduction

Zinc oxide ZnO is a semiconductor material belonging to the transparent conductive oxide (TCO) family. ZnO exhibits unique optoelectronic properties, enabling it to work in photovoltaic applications. As an oxide, it has certain advantages over  $\text{In}_2\text{O}_3$  or ITO, such as being neither combustible nor explosive in the event of a fire or being relatively inert toward the human organism [1]. ZnO is assigned to the group of II-VI semiconductors. It is an intrinsic n-type semiconductor with an exciton binding energy of 60 meV and a wide bandgap equal to 3.37 eV at room temperature [2]. In application research disciplines dealing with TCO [3], thin film gas sensors [4], biomedicine [5], and solar cells [6], these qualities are necessary. In its natural state, ZnO includes a high electron concentration of around  $10^{21} \text{ cm}^{-3}$  [7]. Furthermore, native imperfections such as oxygen vacancies ( $\text{V}_\text{O}$ ) and interstitial zinc cations ( $\text{Zn}_\text{i}$ ) substantially influence its conductivity type [8-10].

However, controlling ZnO's p-type remains a major challenge for ZnO-based devices. This difficulty is also remarkable in GaN, ZnS, CdS, and ZnSe, wide bandgap semiconductors [11]. There are several reasons for the challenges of obtaining p-type doping and conductivity, such as the existence of significant amounts of residual donor-type impurities [12,13], the phenomena of acceptor self-compensation by native n-type defects [7,11,12], the low solubility of potential dopants [11,12,14], the high ionization energy of most potential dopants and the instability of certain dopants within the crystal lattice [12,11]. Various ions may be utilized to dope ZnO,

depending on the specific application. Conductive ZnO films are often doped with elements from the periodic table's group IIIa (Al, In, Ga etc.). However, the effect of these dopants on their various physical features is not well understood. Sol-gel polycrystalline ZnO films doped with copper receive particular attention. This is because Cu and other probable anion dopants, such as halides of this material, have not been thoroughly studied. Copper is a good candidate for substituting zinc sites because its atomic radius of 135 pm is close to zinc [15]. Therefore, one can assume that the ZnO lattice will not or very slightly be deformed by the insertion of copper into the matrix. Thus, it can reduce the concentration of carriers in n-type ZnO by working as a compensation center [16]. Spray deposition [17,18], thermal evaporation [19,20], sputtering [21,22], and sol-gel [23,24] techniques have all been used to create doped ZnO and undoped ZnO thin films. Among them, the sol-gel method was chosen in this work because of its easy use, rapidity, costless, and appropriateness for surface treatment and coating.

Furthermore, it is also possible to deposit thin films of diverse forms with excellent doping control using the sol-gel method. The present study used the sol-gel chemical methodology of the elaborated ZnO thin films and decorated them with different copper concentrations. The deposited samples' characterization was conducted to study their optical, structural, and morphological characteristics.

## 2. Materials

The zinc acetate dihydrates ( $\text{ZnAc}$ ,  $\text{Zn}(\text{CH}_3\text{COO})_2 \cdot 2\text{H}_2\text{O}$ , Sigma-Aldrich, 99.99% trace metal elements) was used as the main precursor, while the solvent was ethanol ( $\text{C}_2\text{H}_5\text{OH}$ , CARLO ERBA Reagents, 99.9%) and ethanolamine (MEA,  $\text{C}_2\text{H}_7\text{NO}$ , Sigma-Aldrich, purity  $\geq 99.0\%$ ) was employed as a sol stabilizer for the formation of the films.

## 3. Methods

Initially, 0.4 M of  $\text{ZnAc}$  was thoroughly dissolved in 20 mL of absolute ethanol. Then, MEA was added to the mixture by a 1:1 molar ratio according to the amount of  $\text{ZnAc}$ . The sol reaction was kept for one hour at  $50^\circ\text{C}$  under continuous stirring to obtain a clear and homogeneous coating solution. To incorporate copper in the film, copper acetate monohydrate ( $\text{CuAc}$ ,  $\text{Cu}(\text{CH}_3\text{COO})_2 \cdot \text{H}_2\text{O}$ , Sigma-Aldrich, purity 99.9%) was added to the starting solution in the molar ratio  $[\text{Cu}/\text{Zn}]$  to get a different concentration of 1, 3, 5, 7 and 10 mol%. The samples were denoted as  $\text{ZnO}$ ,  $\text{CZO1}$ ,  $\text{CZO3}$ ,  $\text{CZO5}$ ,  $\text{CZO7}$ , and  $\text{CZO10}$ . As a pretreatment, the glass substrates were cleaned with ethanol and acetone under ultrasound for 15 min, followed by a water wash and drying. Afterward, the prior coating sols were added dropwise onto the glass substrate ( $1\text{cm} \times 1\text{cm}$ ) and rotated at 3500 rpm for 35 s using a spin coater (Model WS-650 Hz). To evaporate the solvent, the spin-coated substrate was placed in a furnace at  $150^\circ\text{C}$  for 10 min. To reach the target film thickness of 200 nm, this procedure (coating and drying) was done ten times. Finally, the as deposited thin films were calcined at  $600^\circ\text{C}$  in static air for 90 minutes to remove the residual organic element and crystallize the amorphous phase. The prepared thin films were denoted as follows:  $\text{ZnO}$  for reference film and  $\text{CZO}_x$  for Cu-doped  $\text{ZnO}$ , where  $x$  is the  $[\text{Cu}/\text{Zn}]$  mole ratios: 1, 3, 5, 7, and 10 mol%. The structural properties and lattice parameters of  $\text{ZnO}$  and  $\text{CZO}$  films were investigated by the X-ray diffraction method (XRD) on a Bruker D8 Advance X-ray diffractometer with a  $\text{Cu K}\alpha$  anode ( $\lambda = 1.5418 \text{ \AA}$ ). The surface morphology of the films was observed by Scanning Electron Microscopy (SEM), which was carried out using VEGA 3 TESCAN microscope. The optical measurements were realized on a Shimadzu UV-3101PC Spectrophotometer from 250 to 2200 nm, where a blank glass substrate served to set the baseline. The thickness of undoped and doped  $\text{ZnO}$  thin films was around 200 nm. It was verified using a Taylor Hobson profilometer with a resolution of 16 nm.

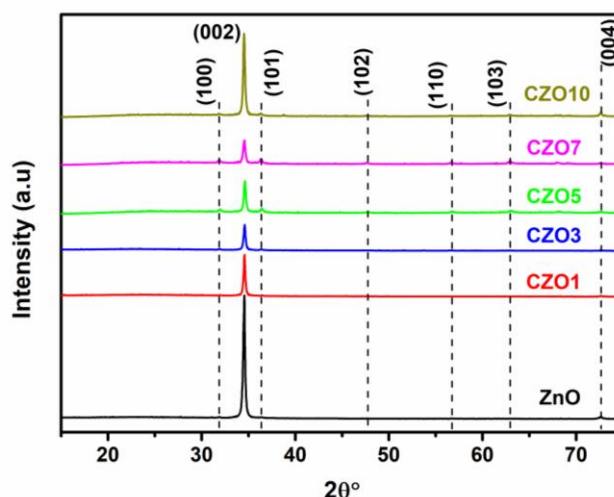


Fig. 1. XRD diffractograms of  $\text{ZnO}$  and Cu-doped  $\text{ZnO}$  thin films (color online)

## 4. Results and discussion

### 4.1. Structural and morphological properties

The diffractograms of  $\text{ZnO}$  and  $\text{CZO}$  thin films are presented in Fig. 1. All the prepared films correspond to the wurtzite-type hexagonal structure of  $\text{ZnO}$  (JCPDF 36-1451) and exhibit a strong preferred c-axis orientation perpendicular to the substrate. Indeed, the main peak is located at  $2\theta = 34.5^\circ$  and is assigned to (002) plane, whereas two other peaks at  $31.9^\circ$  and  $36.35^\circ$  with a lower intensity correspond to (100) and (101), respectively. According to Amirhaghi et al. [25], c-axis privileged orientation may have originated from easier growth along the c-axis as a consequence of the maximum atomic density present in the (002) plane. No additional peaks of  $\text{Cu}$ ,  $\text{CuO}$ , or  $\text{CuO}_2$  are detected, indicating the substantiation of  $\text{Zn}$  with  $\text{Cu}$  into the wurtzite structure. The copper was well substituted into  $\text{Zn}$  sites without changing the polycrystalline structure. Comparing  $\text{CZO}$  to  $\text{ZnO}$  films, the (002) diffraction peak's intensity falls clearly following as the doping content increases to 7%  $\text{Cu}$ . For 10%  $\text{Cu}$ , the intensity of (002) exhibits the same intensity as the undoped  $\text{ZnO}$ .

The decrease of the peak intensity can be due to the deterioration of crystallinity with  $\text{Cu}$  incorporation [26]. Similar findings have been noted [27]. However, Lee et al. [28] noticed that copper doping increased the degree of the c-orientation.

The mean crystallite size ( $D$ ) of  $\text{ZnO}$  and  $\text{CZO}$  thin films was estimated using the well-known Debye-Scherrer equation based on the location of the (002) principal reflection and its FWHM. Fig. 2 shows the variation of (FWHM) of the (002) peak and the corresponding ( $D$ ) versus the copper content. It seems that FWHM reaches a maximum of 5%  $\text{Cu}$ . According to the Williamson-Hall formula [29], strain and mean crystallite size have an inverse effect on FWHM. Then, given that the crystallite size ( $D$ ) decreases as the copper ratio up to 5 mol%, the

drop in the (002) diffraction peak may be attributed principally to an increase in film strain. Furthermore, the decrease of crystallite size from 55.07 nm (CZO1) to 32.13 nm (CZO5) can be attributed to the variation in ionic radii of the dopant,  $r(\text{Cu}^{2+}) = 0.57 \text{ \AA}$  and  $r(\text{Zn}^{2+}) = 0.74 \text{ \AA}$  [30], which makes the CuZn-O bond shorter in substantial doping. It can also be explained by the effects of stresses, which originate from the films' different thermal expansion coefficients,  $\alpha(\text{ZnO}) = 7.10 \cdot 10^{-6} \text{ }^\circ\text{C}^{-1}$  and  $\alpha(\text{glass}) = 4.10 \cdot 10^{-6} \text{ }^\circ\text{C}^{-1}$  [31]. The increase in the crystallite size to 35 nm for (CZO10) can be explained by the incorporation of  $\text{Cu}^+$  cation in the interstitial sites at a high concentration of dopant due to the large ionic radii of  $\text{Cu}^+$  (0.96 Å) compared to  $\text{Zn}^{2+}$  (0.74 Å) [30].

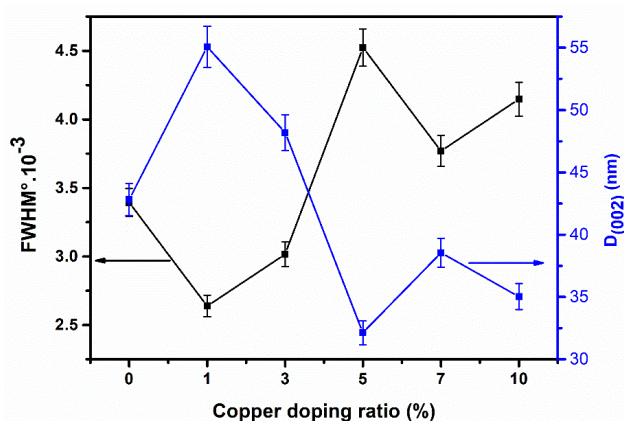


Fig. 2. Crystallite size and FWHM data analysis of the different samples (color online)

The surface morphologies of ZnO and CZO thin films prepared at different concentrations of copper are shown in Fig. 3. It is proved that as the concentration of copper content is changed, the surface morphology of CZO films changes. The nanostructured thin films are dense and show an increasingly smooth surface with copper doping. On the other hand, the diameter of the nanowires depends on the copper concentration; it decreases with the doping rate. This result agrees with the results observed by the XRD analysis. This is similar to other findings in references [30, 32]. The average length of the nanowires was 0.5  $\mu\text{m}$ .

#### 4.2. Optical properties

The UV-vis spectra of ZnO and CZO samples are presented in Fig. 4. All the films were highly transparent in the visible region. All spectra show two regions: a region of strong absorption at [360-400 nm], corresponding to the intrinsic absorption in films (interband transition). The second region of high transparency [400-800 nm] with an average maximum value of 90 % for the CZO3 sample. The transmittance decreases at higher doping content (5%, 7%, and 10%). One also notes the absence of interference fringes in all transmission spectra. This degradation of transmittance and the absence of interference fringes can be assigned to numerous random scatterings of the incident light between the inter-column voids, the c-axis oriented nanowires

(orientation (002)), and some tilted nanowires which are not well aligned vertically from the CZO5 sample (appearance of the (100) and (101) orientations on the XRD spectra) [30]. The origin of the transmittance degradation could also be structural; when the copper is in interstitial sites, there is an increase in the compactness of the lattice, and consequently, the transmittance decreases. Another explanation for transmittance degradation is cited by Payan and Rassigni, where certain transition metals, such as copper, exhibit abnormal absorption in the visible range [33-35]. One can conclude that at higher content of Cu, the insertion of Cu dopant into the ZnO lattice leads to poor transmittance.

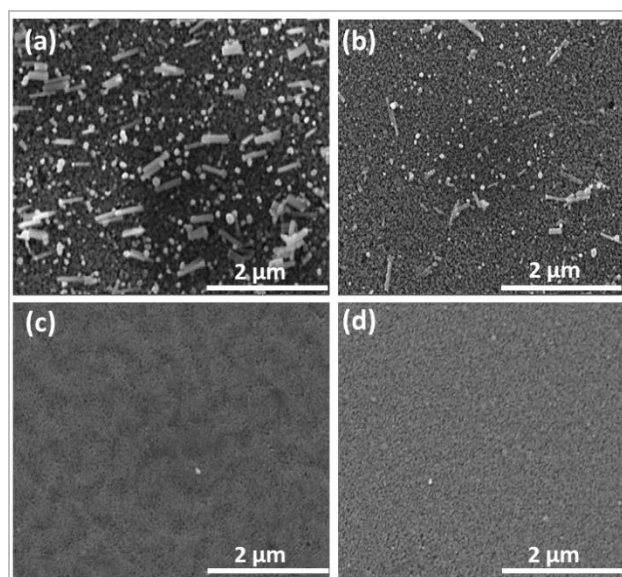


Fig. 3. SEM images of ZnO and CZOx thin films (a) ZnO, (b)  $x = 3\%$ , (c)  $x = 7\%$ , (d)  $x = 10\%$

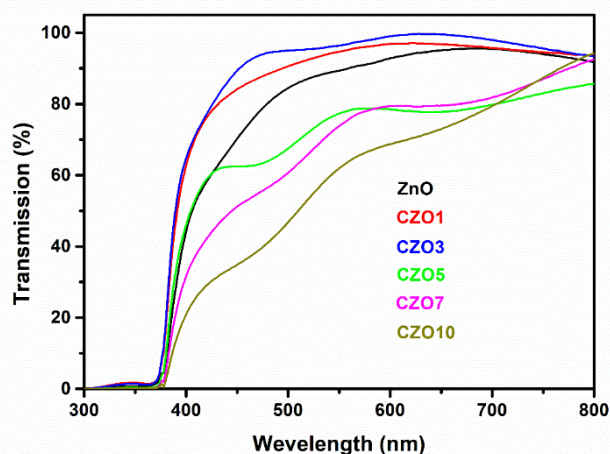


Fig. 4. Transmission spectra of ZnO and CZO thin films (color online)

The optical bandgap ( $E_g$ ) of ZnO and CZO films was evaluated by using the equation (1) below and presented in

$$\alpha \cdot hv = A \cdot (hv - E_g)^{1/2} \quad (1)$$

where  $h\nu$  is the photon energy,  $\alpha$  is the absorption coefficient, and  $A$  is an energy-independent factor. The optical bandgap was deduced by intercepting the linear component of the absorption curve,  $(\alpha \cdot h\nu)^2$  on the Y-axis, with the photon energy on the X-axis (Fig. 5-inset). The strong absorption edge of undoped ZnO is located at 381 nm (3.2 eV), which is quite near to the intrinsic bandgap of ZnO. This result was consistent with the values mentioned in the literature. One can distinguish two regions,  $\text{Cu} < 5\%$  (bleu shift), the  $E_g$  increases proportionally with copper concentration and  $\text{Cu} \geq 5\%$  (red-shift), where increasing dopant ratio, the bandgap energy decreases. The enlargement of the bandgap energy ( $\text{Cu} < 5\%$ ) is interpreted by the Burstein-Moss effect [36,37]. According to the latter, as the doping level rise, the optical bandgap shifts toward the blue region (bleu-shift). This effect is caused by the increase in the density of charge carriers originating mainly from the interstitial zinc atoms ( $\text{Zn}_i$ ) or the oxygen vacancies ( $\text{O}_v$ ) at ambient temperature [32-38]. However, the observed red-shift ( $\text{Cu} \geq 5\%$ ) can be associated to the apparition of an energy ionic level of  $\text{Cu}^+$  in the bandgap [32].

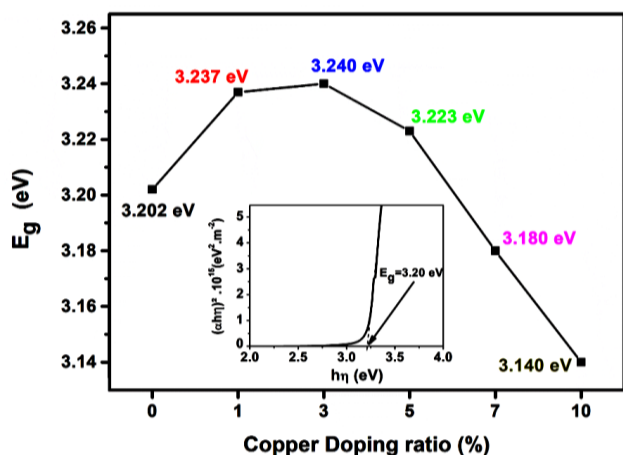


Fig. 5. ZnO optical band gap Vs Cu doping ratio. Inset: example of band gap determination of undoped ZnO (color online)

The determination of the extinction coefficient ( $k$ ), which represents the energy loss of electromagnetic radiation, and the refractive index ( $n$ ) were calculated using the following equations (2) and (3), respectively. The values and variation of  $n$  and  $k$ , at 500 nm, are presented in Table 1 and Fig. 6, respectively.

$$k = \alpha \lambda / 4\pi \quad (2)$$

$$n = [(2-T)/T] + [((4*(1-T))/(2*T) - k^2)]^{1/2} \quad (3)$$

Table 1.  $n$  and  $k$  for ZnO thin films doped with different Cu concentrations at 500 nm

	ZnO	CZO1	CZO3	CZO5	CZO7	CZO10
$k$	0.03	0.02	0.01	0.07	0.10	0.15
$n$	1.98	1.66	1.42	2.93	3.44	4.78

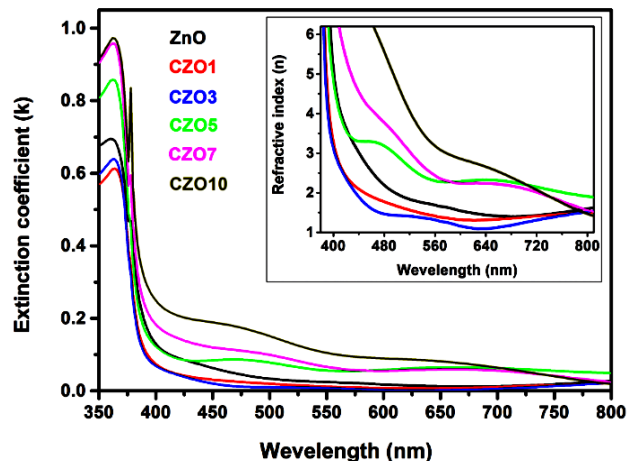


Fig. 6. Extinction coefficient ( $k$ ) and (inset) refractive index ( $n$ ) for ZnO and CZO thin films (color online)

In Table 1, the low  $k$  and  $n$  in the visible range explain the high transparency of all prepared thin films. The value of the refractive index of ZnO massive is 2. In the thin film domain, the refractive index ( $n$ ) and the absorption coefficient ( $\alpha$ ) vary according to the conditions of the preparation of the layers [39]. In general, the refractive index of TCOs, case of ZnO and CZO, is between 1.7 and 2.2 for visible wavelengths [40,41].

## 5. Conclusion

A sol-gel route and spin-coating process were adopted to prepare nanostructured thin films of undoped and copper-doped ZnO (CZO) with different content. The effect of Cu doping on the structural, morphological, and optical behaviors was investigated. All the films exhibited interesting crystallographic characteristics and a privileged c-axis orientation along the (002) direction. The crystallite size varies from 32 nm to 55 nm, suggesting that Cu and the preparation process directly influence the structural characteristics of CZO films. The optical properties in all samples show high transparency of ZnO and CZO thin films with different copper doping content.

Additionally, at 5 % of Cu, one can mention two distinct regions where the variation of all investigated parameters changes oppositely. Consequently, at a higher Cu doping rate (above 5 % of Cu), the structural and optical features of the films deteriorate, which is the opposite in the low Cu doping region. The highly transparent ZnO thin films and probably highly conductive, doped with Cu at a concentration of 3 mol%

(where  $E_g = 3.240$  eV), may be helpful in optoelectronic applications requiring a large surface area.

## References

- [1] A. Taabouche, PhD thesis, University of Frères Mentouri Constantine, Algeria, 2015.
- [2] Ü. Özgür, Ya. I. Alivov, C. Liu, A. Teke, M. A. Reshchikov, S. Doğan, V. Avrutin, S.-J. Cho, H. Morkoç, *J. Appl. Phys.* **98**, 041301 (2005).
- [3] I. Y. Y. Bu, *Superlattices and Microstructures* **60**, 160 (2013).
- [4] I. Y. Y. Bu, C. C. Yang, *Superlattices and Microstructures* **51**, 745 (2012).
- [5] S. Singh, P. Chakrabarti, *Superlattices and Microstructures* **64**, 283 (2013).
- [6] S. H. Jeong, B. N. Park, D. G. Yoo, J. H. Boo, *J. Korean Phys. Soc.* **50**, 622 (2007).
- [7] J. C. Fan, K. M. Srekanth, Z. Xie, S. L. Chang, K. V. Rao, *Prog. Mater. Science* **58**, 874 (2013).
- [8] K. Punia, G. Lal, Satya N. Dolia, S. Kumar, *Ceram. Int.* **46**, 12296 (2020).
- [9] B. Huang, *Solid State Commun.* **237-238**, 34 (2016).
- [10] M. A. Lahmer, K. Guergouri, *Material Science in Semiconductor Processing* **39**, 148 (2015).
- [11] H. Morkoç, Ü. Özgür, *Zinc Oxide: Fundamentals, Materials and Device Technology*, Wiley-VCH, Germany, 2009.
- [12] S. Brochen, PhD thesis, University of Grenoble, France, 2012.
- [13] A. Janotti, C. G. Van de Walle, *Rep. Prog. Phys.* **72**, 126501 (2009).
- [14] I. Y. Y. Bu, *Superlattices and Microstructures* **96**, 59 (2016).
- [15] <http://www.elementschimiques.fr>, accessed 20 Mars 2022.
- [16] R. Vettumperumal, S. Kalyanaraman, R. Thangavel, *Superlattices and Microstructures* **83**, 237 (2015).
- [17] R. Grothe, S. Knust, D. Meinderink, M. Voigt, A. González Orive, G. Grundmeier, *Surf. Coat. Technol.* **394**, 125869 (2020).
- [18] J. L. Bubendorff, J. Ebothé, A. El Hichou, R. Dounia, M. Addou, *J. Appl. Phys.* **100**, 014505 (2006).
- [19] N. Sheeba, S. C. Vattappalam, G. Okram, V. Sharma, P. Sreenivasan, S. Mathew, R. Reena Philip, *Mater. Res. Bull.* **93**, 130 (2017).
- [20] N. F. H. Siti, A. A. H. Muhammad, S. Roslinda, J. Azman, *J. Phys. Chem. Sol.* **70**, 1501 (2009).
- [21] Y. Andolsi, F. Chaabouni, *J. Alloys Compd.* **818**, 152739 (2020).
- [22] R. S. Gonçalves, P. Barrozo, G. L. Brito, B. C. Viana, F. Cunha, *Thin Solid Films* **661**, 40 (2018).
- [23] D. Ali, M. Z. Butt, I. Muneer, M. A. Farrukh, M. Aftab, M. Saleem, F. Bashir, A. U. Khan, *Thin Solid Films* **679**, 86 (2019).
- [24] M. Caglar, Y. Caglar, S. Aksoy, S. Ilcan, *Appl. Surf. Sci.* **256**, 4966 (2010).
- [25] S. Amirhaghi, V. Craciun, D. Craciun, J. Elders, I. W. Boyd, *Microelectron. Eng.* **25**, 321 (1994).
- [26] M. Caglar, F. Yakuphanoglu, *Appl Surf Sci.* **258**, 3039 (2012).
- [27] A. E. Jiménez-González, *J. Solid State Chem.* **128**, 176 (1997).
- [28] J. B. Lee, H.-J. Lee, S.-H. Seo, J.-S. Park, *Thin Solid Films* **398-399**, 641 (2001).
- [29] J. S. Wellings, N. B. Chaure, S. N. Heavens, I. M. Dharmadasa, *Thin Solid Films* **516**, 3893 (2008).
- [30] M. Babikier, D. Wang, J. Wang, Q. Li, J. Sun, Y. Yan, Q. Yu, S. Jiao, *Nanoscale Res. Lett.* **9**, 199 (2014).
- [31] F. A. Humánez, O. Almanza, C.V. Hernández, *Superf. vacío* **27**, 43 (2014).
- [32] M. Chakraborty, A. Ghosh, R. Thangavel, *J. Sol-Gel Sci. Technol.* **74**, 756 (2015).
- [33] R. Payan, G. Rassigni, *J. Phys. France* **25**, 92 (1964).
- [34] T. Minami, S. Suzuki, T. Miyata, *Thin Solid Films* **398-399**, 53 (2001).
- [35] N. Emeric, A. Emeric, R. Philip, *Journal de Physique* **26**, 769 (1965).
- [36] T. S. Moss, *Proc. Phys. Soc. B* **67**, 775 (1954).
- [37] E. Burstein, *Phys. Rev.* **93**, 632 (1954).
- [38] Z. B. Bahşi, A. Y. Oral, *Opt. Mater.* **29**, 672 (2007).
- [39] M. Maache, PhD thesis, University of Mohamed Khider, Algeria, 2014.
- [40] J. Garnier, PhD thesis, Arts et Métiers ParisTech, France, 2009.
- [41] G. K. L. Goh, S. K. Donthu, P. K. Pallathadka, *Chem. Mater.* **16**, 2857 (2004).

\*Corresponding author: h.elmarouazi@gmail.com